separations

MDPI

Article

Vapor–Liquid Equilibrium and Design of Energy-Efficient High-Vacuum Pressure-Swing Distillation for Bio-Based Alcohol/Alkane Separation

Chunli Li [1], Tianzhu Ma [1], Yuze Sun [1], Kaile Shi [1], Wen Liu [2,*], Rui Wang [3,*] and Jiapeng Liu [1,*]

[1] National and Local Joint Engineering Laboratory for Integrated Energy Saving in Chemical Industry and Resource Utilization, College of Chemical Engineering, Hebei University of Technology, Tianjin 300130, China; lichunli_hebut@126.com (C.L.); matianzhu1999@163.com (T.M.); syz17546411218@163.com (Y.S.); skl20001105@163.com (K.S.)
[2] College of Basic Science, Tianjin Agricultural University, Tianjin 300392, China
[3] School of Chemistry & Chemical Engineering, Tianjin University of Technology, Tianjin 300384, China
* Correspondence: liuwen@tjau.edu.cn (W.L.); wrui@tju.edu.cn (R.W.); liujiapeng@hebut.edu.cn (J.L.)

Abstract

Fatty alcohols and aliphatic hydrocarbons occur abundantly in nature and serve as critical feedstocks for the surfactant and fuel industries, respectively. However, their industrial-scale separation and purification are significantly hampered by high boiling points and the formation of complex azeotropes. To address these challenges, this study explores a five-column high-vacuum pressure-swing distillation (HVPSD-5C) strategy. Vapor–liquid equilibrium (VLE) analysis of the key components (n-hexanol, n-octanol, n-dodecane, and n-tridecane) validated the thermodynamic viability of the process and established optimal operating conditions. To further enhance efficiency, a heat-pump-integrated configuration (HPI-HVPSD-5C) featuring vapor recompression and heat integration was designed, optimized, and evaluated. Comparison with the baseline HVPSD-5C process demonstrates that the HPI-HVPSD-5C configuration significantly improves sustainability and economics, reducing the total annual cost (TAC) by 17.48%, CO_2 emissions by 16.09%, and energy consumption cost by 12.79%. These findings provide a robust framework for the efficient separation of fatty alcohols from aliphatic hydrocarbons, offering a valuable reference for the purification of other pressure-sensitive azeotropic mixtures.

Keywords: fatty alcohols; vapor–liquid equilibrium; pressure-swing distillation; heat integration; separation and purification

Academic Editor: Hideo Maruyama

Received: 4 April 2026
Revised: 6 May 2026
Accepted: 16 May 2026
Published: 18 May 2026

1. Introduction

Fatty alcohols are obtained from natural oils and fats via high-pressure hydrogenation [1], yielding valuable components including n-hexanol, n-octanol, n-dodecane, and n-tridecane, which are widely used in solvents, food, fuels, and other fields [2–7]. However, due to the high boiling points of n-octanol and n-dodecane and their tendency to form azeotropes, conventional distillation is ineffective for their separation. Therefore, achieving efficient separation is of great significance.

The separation task arises from an industrial fatty alcohol process based on high-pressure hydrogenation of natural oils. The feed, supplied by an enterprise, consists of 8.0 wt% n-hexanol, 82.0 wt% n-octanol, 8.0 wt% n-dodecane, and 2.0 wt% n-tridecane. The goal is to recover n-octanol at $\geq$99.5 wt% purity and to achieve > 99.0 wt% purity for each of the other three components, enabling their reuse or further treatment.

Advanced distillation methodologies—including azeotropic [8], extractive [9], reactive [10], and pressure-swing distillation [11] (PSD)—have been developed for bypassing azeotropic constraints. Among these, pressure-swing distillation is particularly advantageous, as it circumvents the need for external entrainers or solvents, thereby eliminating the risks of product contamination and the additional costs associated with solvent recovery. Given that the n-octanol/n-dodecane azeotropic composition is highly sensitive to pressure changes, PSD emerges as the most suitable candidate for this system. Consequently, this study focuses on the exploration of high-vacuum pressure-swing distillation (HVPSD), which not only enables effective separation but also operates at lower temperatures to prevent thermal degradation of these high-boiling-point components. In Hanbin Wu et al.'s [12] study, the ternary azeotrope (1,4-dioxane/water/ethyl acetate) was successfully separated by combining azeotropic distillation with self-heat-recovery technology. Experimental results show high product purity and a 64.28% reduction in total energy consumption. Baoming Shan et al. [13] successfully separated a toluene–methanol–water ternary azeotrope using extractive distillation with glycerol, an efficient and environmentally friendly solvent. Currently, researchers [14] are utilizing supercritical fluids (such as CO_2) as solvents to separate alcohols and alkanes (C8-C20) based on differences in solubility under supercritical conditions [15]. Other researchers [16] have employed extractive distillation to separate mixtures of undecane, dodecane, and 1-decanol, using ionic liquids as an extracting agent. However, the rigorous design and optimization of such processes are often hindered by the lack of reliable thermodynamic data. High-quality experimental vapor–liquid equilibrium (VLE) data under high-vacuum conditions are notably scarce in the open literature. Precise VLE data and accurately regressed binary interaction parameters are essential precursors for constructing a dependable simulation model and determining the optimal pressure-swing range. To further enhance the thermodynamic efficiency of the process, process intensification through heat integration—specifically vapor recompression and heat-pump-assisted distillation—has emerged as a powerful strategy [17]. By upgrading low-grade heat from the condenser for reuse in the reboiler, these technologies can significantly reduce the external utility requirements and the overall carbon footprint of the distillation sequence.

This study aims to develop and intensify an energy-efficient high-vacuum pressure-swing distillation (HVPSD) process for separating a complex quaternary system of fatty alcohols and alkanes. After validating the thermodynamic framework via experimental VLE measurements and molecular interaction analysis, a baseline HVPSD sequence was optimized to minimize Total Annual Cost (TAC). Process intensification was then achieved through heat-pump integration and vapor recompression, significantly reducing energy intensity. The resulting configurations were comprehensively evaluated, demonstrating substantial improvements in economic viability and CO_2 emission reduction compared to the conventional process.

2. Experimental and Methods

2.1. Experimental Chemicals

n-hexanol (≥99.0 wt%) and n-octanol (≥99.0 wt%) were purchased from China Shanghai Macklin Biochemical Technology Co., Ltd. (Shanghai, China); n-dodecane (≥99.0 wt%) and n-tridecane (≥99.0 wt%) were purchased from China Shanghai Dibai Chemical Co., Ltd. (Shanghai, China).

2.1.1. VLE Experimental Apparatus and Procedure

The experiment was conducted using a modified Othmer still [18] with validated reliability (Figure 1). The apparatus is equipped with vapor and liquid sampling ports, a

heating rod, a vacuum pump, a pressure gauge, heating tape, and a condenser. Pressure was measured by a vacuum gauge with an accuracy of 0.0001 bar, and the equilibrium temperature was measured by a mercury thermometer with an accuracy of 0.01 °C. Both phases were continuously circulated until stable temperature and pressure indicated equilibrium. Samples were then withdrawn using a micro-syringe for analysis.

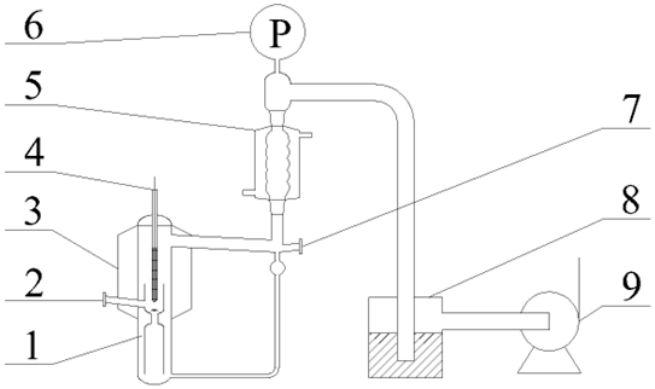

Figure 1. Vapor–liquid phase equilibrium device. 1. Heating chamber; 2. liquid-phase sampling port; 3. vacuum insulation sleeve; 4. temperature-measurement tube; 5. condenser tube; 6. high-vacuum gauge; 7. gas-phase sampling port; 8. absorption buffer tank; and 9. high-vacuum pump.

Vapor–liquid equilibrium (VLE) data (Tables A1–A6) were measured at 1.0 kPa for the binary systems: n-hexanol/n-octanol, n-hexanol/n-dodecane, n-hexanol/n-tridecane, n-octanol/n-dodecane, n-octanol/n-tridecane, and n-dodecane/n-tridecane. Data for n-octanol/n-dodecane, n-octanol/n-tridecane, and n-dodecane/n-tridecane were additionally obtained at 50.0 kPa [19–22]. Samples were withdrawn using a micro-syringe for analysis.

2.1.2. Analytical Methods

Vapor and liquid compositions were analyzed by gas chromatography (GC) with 0.4 μL samples. The analytical method is detailed in Table A7.

2.2. Molecular Simulation

Intermolecular interactions were calculated using density functional theory (DFT) in Gaussian 16 [23]. Calculations were performed at the B3LYP-D3BJ/TZVP level to optimize molecular structures and complexes, with local energy minima confirmed by positive vibrational frequencies. The interaction energy (E_{inter}) was derived from Equation (1) [24], as the difference between the energy of the complex and the sum of the monomer energies:

$$E_{inter} = E_{AB} - E_A - E_B \quad (1)$$

In Equation (1), E_{AB} corresponds to the total energy of the complex between components A and B, whereas E_A and E_B refer to the energies of the isolated monomers. The mixing energy change was then computed with Equation (2) [24].

$$\Delta E = 2E_{AB} - E_{AA} - E_{BB} \quad (2)$$

If the calculated value of ΔE (the intermolecular interaction energy) is zero, the system is considered to exhibit ideal mixing behavior. Conversely, a significant deviation of ΔE from zero indicates a substantial departure from ideal behavior [25].

2.3. Process Optimization Method Process Design and Optimization

All simulations and optimizations were performed using Aspen Plus V11. The feed to the quaternary mixture of n-hexanol, n-octanol, n-dodecane, and n-tridecane was set to 1000.0 kg/h, with individual mass flow rates of 80.0, 820.0, 80.0, and 20.0 kg/h, respectively, reflecting the composition of an industrial fatty alcohol stream. The feed was introduced at 25.0 °C and atmospheric pressure, and the target purity for each product was ≥99.5 wt%.

Processes were optimized with the objective of minimizing the TAC using a sequential optimization method (Figure 2) [26,27]. Distillation columns were modeled with the RADFRAC module, and both the distillate flow rate and reflux ratio of each column were adjusted to meet the specified targets. The optimization variables are five operating pressures (P_1–P_5), five total theoretical stages (N_{S1}–N_{S5}), and five feed stage locations (N_{f1}–N_{f5}).

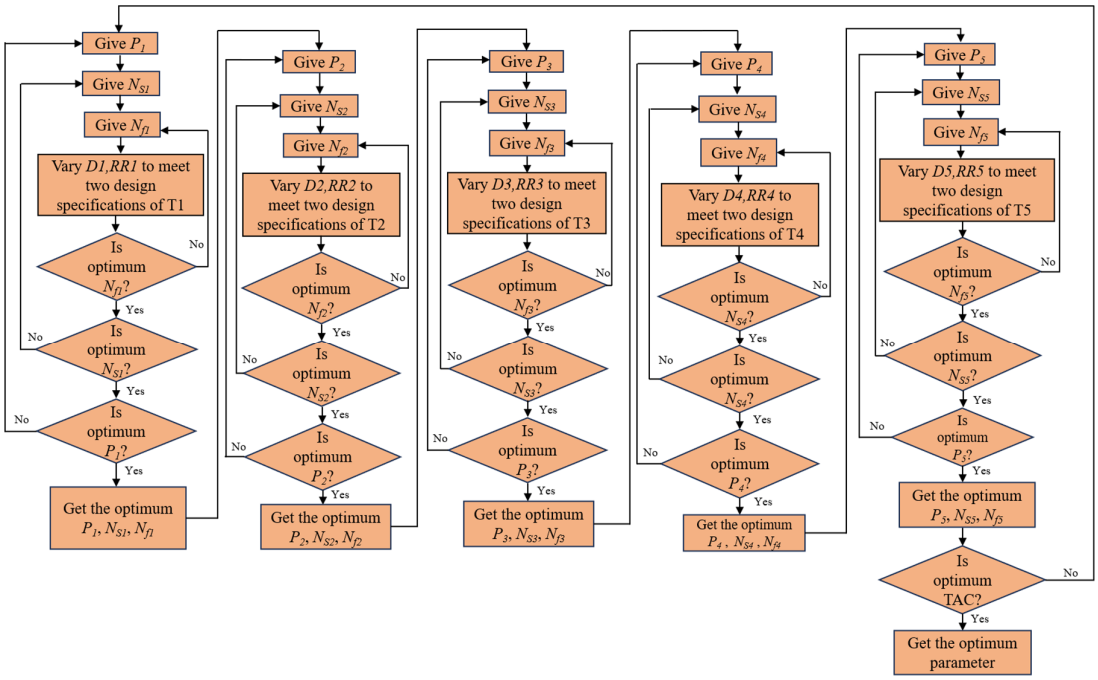

Figure 2. Five-column high-vacuum pressure-swing distillation (HVPSD-5C) process sequence iterative optimization flowchart.

2.4. Process Evaluation

2.4.1. Economic Analysis

All process parameters were selected based on economic feasibility. Following the method of Douglas [28], the process simulation was optimized with the goal of minimizing TAC, which is calculated as follows:

$$TAC = OC + \frac{FCI}{P} \tag{3}$$

Operating costs (*OC*) include cooling utilities and steam expenses. Fixed Capital Investment (*FCI*) covers the costs of the distillation column shell, column internals (sieve trays), and heat exchangers (condenser and reboiler) [17]. Auxiliary components such as pumps, valves, and piping are omitted due to their relatively low impact on overall costs [29]. Thus, *FCI* consists of four major components: the column vessel, internals sieve trays, condenser, and reboiler.

A payback period of 5 years is assumed, with an annual operating time of 8000 h. Equipment costs are estimated using the 2018 Marshall & Swift (M&S) index of 1638.2 [30].

The vacuum system cost is calculated following the method of Seider et al. [31], with pump power determined from an isentropic compressor model assuming an isentropic efficiency of 0.4 and a mechanical efficiency of 0.92. The corresponding equations are provided in Table A8.

2.4.2. Energy Assessments

Key factors influencing total energy consumption (Q_{total}, kW) are primarily the reboiler heat duty (Q_W, kW) and electricity consumption by vacuum pumps. Owing to considerations of thermoelectric conversion efficiency, thermal energy is valued at three times the equivalent amount of electrical energy [32]. The computation of the total energy consumption utilized the following Equation (4):

$$Q_{total} = Q_W + 3P \tag{4}$$

2.4.3. CO_2 Emission Assessment

CO_2 emissions are primarily attributed to the steam utility consumed in reboilers, representing a critical environmental impact factor [33]. Since steam is generated via combustion in boilers, the associated CO_2 emissions are calculated according to [34] using the methodology specified in Equation (5):

$$[CO_2]_{Emission} = Q_{Fuel} \times Fuel_{Fact} \tag{5}$$

As expressed in Equation (5), CO_2 emissions are governed by fuel combustion quantity (Q_{Fuel}) and the fuel-specific emission factor ($Fuel_{Fact}$):

$$Q_{Fuel} = \frac{Q_{Proc}}{\lambda_{Proc}}(h_{Proc} - h_{Water,373.15K})\frac{T_{FBI} - T_0}{T_{FBI} - T_{Stack}} \tag{6}$$

In Equation (6), λ_{Proc} (kJ/kg) and h_{Proc} (kJ/kg) represent the latent heat and enthalpy of utility-grade process steam, respectively. T_{FBI} denotes the theoretical adiabatic flame temperature of 2073.15 K required for the process heat load. In the simulation, the boiler feedwater temperature was assigned a value of 373.15 K, and its corresponding enthalpy was defined as 419 kJ/kg.

$$Fuel_{Fact} = \left(\frac{\alpha}{NHV}\right)\left(\frac{C\%}{100}\right) \tag{7}$$

A molar mass ratio α of 3.67 was adopted for CO_2 to carbon. The simulation utilized heavy fuel oil, which is characterized by a net heating value (NHV) of 39,770 kJ/kg and a carbon content of 86.5 wt%. The NHV represents the carbon energy content of the fuel.

Based on the literature [35], electricity results in CO_2 emissions of 51.1 kg CO_2/GJ. Employing Aspen Plus V11 enthalpy data, the calculated CO_2 emissions were 98.44 kg CO_2/GJ for LP steam and 135.75 kg CO_2/GJ for HP steam, based on Equations (4)–(7).

3. Results and Discussion

3.1. VLE and Binding Energy Results

VLE data for the nine binary systems are provided in Tables A1–A6. The thermodynamic consistency test was conducted using the Herington [36] area method to verify reliability (the relevant calculation formulas are shown in Table A9), and the results are shown in Figure 3 and Table 1. γ_i represents the activity coefficient of component i, with the expression of the activity coefficient shown in Equation (8). P_i^s is the actual operating pressure (atmospheric pressure) and P_i^s is the saturated vapor pressure, as calculated

using the extended Antoine equation, as shown in Equation (9), with parameters shown in Table A10.

$$y_i = \frac{p_i^s \cdot \gamma_i}{p} \cdot x_i \tag{8}$$

$$\ln P = C1 + \frac{C2}{T + C3} + C4 \times T + C5 \times \ln T + C6 \times T^{C7} for C8 \leq T \leq C9 \tag{9}$$

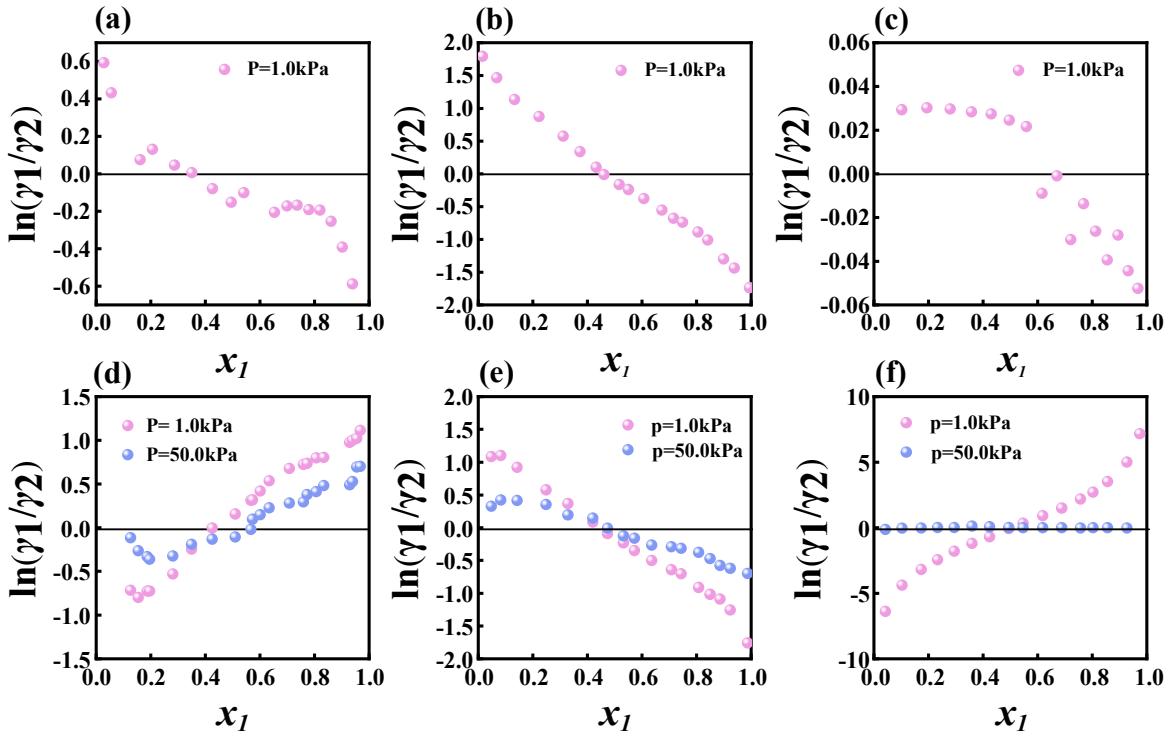

Figure 3. Herrington area method: curve of x_1 versus $\ln(\gamma_1/\gamma_2)$. (**a**) n-hexanol and n-octanol; (**b**) n-hexanol and n-dodecane; (**c**) n-hexanol and n-triacontane; (**d**) n-octanol and n-dodecane; (**e**) n-octanol and n-tridecane; (**f**) n-dodecane and n-tridecane.

Table 1. Thermodynamic consistency test results.

System	P/kPa	T_{max}/K	T_{min}/K	D	J	|D−|
n-hexanol/n-octanol	1.0	356.15	328.35	22.2998	12.6999	9.599
n-hexanol/n-dodecane	1.0	351.15	330.25	1.416	9.493	8.077
n-hexanol-n-tridecane	1.0	361.3	329.95	15.939	14.252	0.687
n-octanol/n-dodecane	1.0	356.85	350.05	11.9318	2.9139	9.017
n-octanol/n-dodecane	50.0	460.75	434.45	18.8697	9.0804	9.789
n-octanol/n-tridecane	1.0	369.95	355.15	15.9407	6.2509	9.689
n-octanol/n-tridecane	50.0	475.00	444.40	13.3607	10.3285	3.032
n-dodecane/n-tridecane	1. 0	373.15	359.35	1.2753	5.7604	4.485
n-dodecane/n-tridecane	50.0	479.85	461.85	0.6183	5.8083	5.190

The |D−J| values for all systems are below 10 (Table 1), confirming that the experimental binary data satisfy the thermodynamic consistency test.

The regression of binary parameters was performed using the NRTL [37–39], UNIQUAC [40], and Wilson [41] activity coefficient models due to their distinct theoretical foundations and complementary strengths. The fitting results are presented in Figure 4.

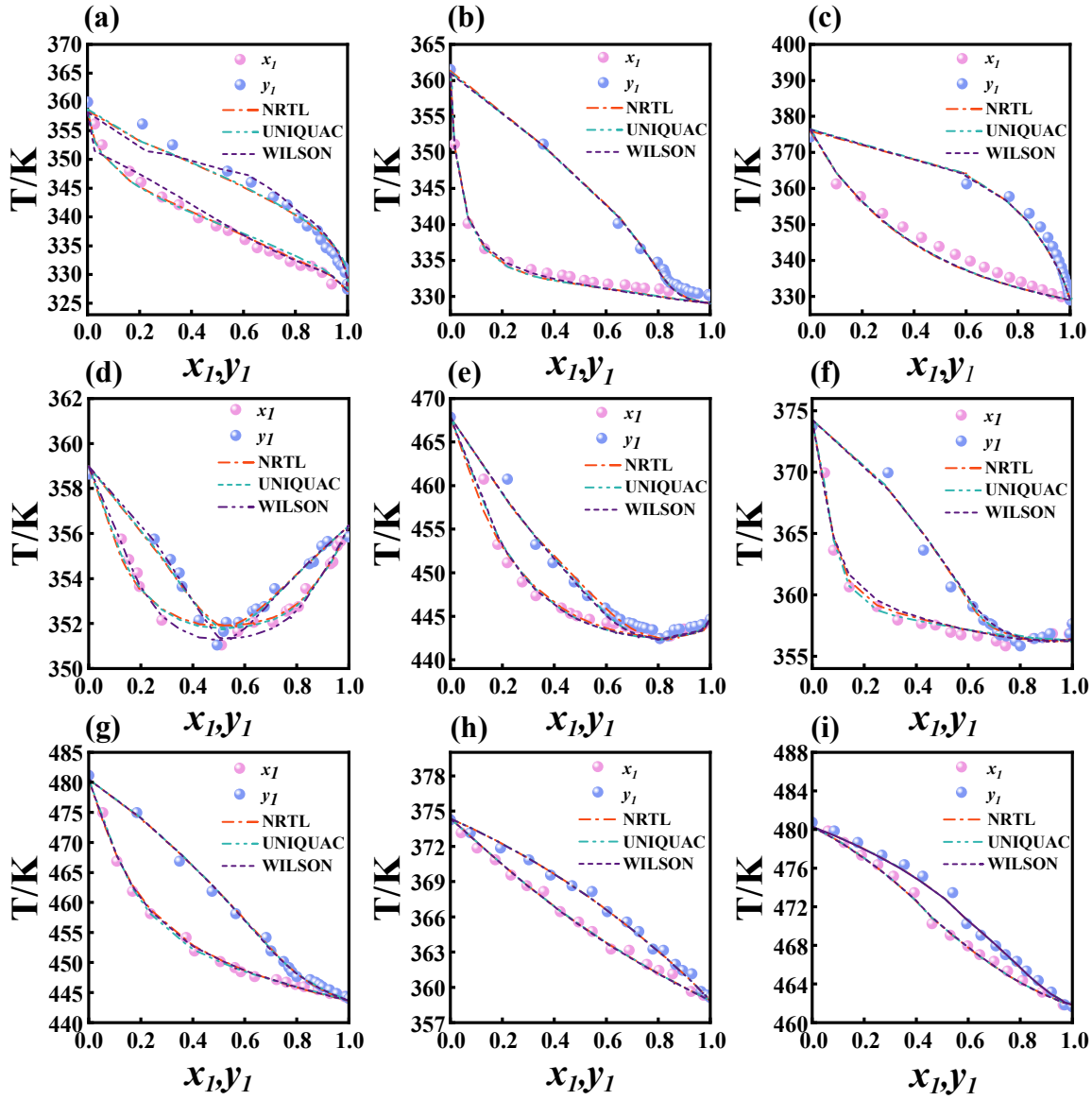

Figure 4. Experimental and predicted T-x_1-y_1 diagram at 1.0 kPa and 50.0 kPa. x_1: Mole fraction of the light component in the liquid phase; y_1: Mole fraction of the light component in the vapor phase. n-hexanol/n-octanol: (**a**) p = 1.0 kPa; n-hexanol/n-dodecane: (**b**) p = 1.0 kPa; n-hexanol/n-tridecane: (**c**) p = 1.0 kPa; n-octanol/n-dodecane: (**d**) p = 1.0 kPa; (**e**) p = 50.0 kPa; n-octanol/n-tridecane: (**f**) p = 1.0 kPa; (**g**) p = 50.0 kPa; n-dodecane/n-tridecane: (**h**) p = 1.0 kPa; (**i**) p = 50.0 kPa.

As shown in Figure 4a–c, the relative volatility of n-hexanol is high under low-pressure conditions, enabling its preferential separation as the light component. Figure 3d,e show that the azeotropic composition of the n-octanol/n-dodecane binary system varies significantly with pressure: 0.51/0.48 at 1.0 kPa and 0.795/0.205 at 50.0 kPa, providing a basis for breaking the azeotrope via pressure-swing distillation. Additionally, Figure 4f–i reveal that the relative volatility at 1.0 kPa is markedly higher than at 50.0 kPa, favoring separation of the quaternary system. Thus, high-vacuum pressure-swing distillation offers a significant thermodynamic advantage for this system.

The NRTL, UNIQUAC, and Wilson equations are all semi-empirical models widely recognized for their high accuracy in predicting VLE behavior. Through the regression of binary interaction parameters, their errors can be confined within an acceptable range for engineering applications, with the average absolute deviation (AAD) typically being less than 1%. The correlation was validated using root mean square deviation (RMSD) and

the average absolute deviation (AAD), as provided in Table A11, with the corresponding calculation equations shown in Table A12.

Analysis of Table A11 and Figure 4 indicates that the NRTL model achieved higher accuracy in representing the binary systems studied. The binary interaction parameters for the NRTL model are listed in Table 2.

Table 2. Binary Interaction Parameters for NRTL.

System	P/kPa	a_{ij}	a_{ji}	b_{ij}	b_{ji}	c_{ij}
n-hexanol/n-octanol	1.0	28.065	−27.485	−10,000.0	10,000.0	0.3
n-hexanol/n-dodecane	1.0	−10.904	13.546	3812.08	−4074.34	0.3
n-hexanol/n-tridecane	1.0	−4.562	−2.424	1874.11	494.872	0.3
n-octanol/n-dodecane	1.0	−1.645	−11.5093	786.759	4328.32	0.3
	50.0	−1.3427	−11.5093	1084.46	5017.75	0.3
n-octanol/n-tridecane	1.0	0.4868	−25.7474	−218.547	10,000.0	0.3
	50.0	−2.2389	−1.2059	1110.25	796.989	0.3
n-dodecane/n-tridecane	1.0	−3.8720	−6.02471	1019.58	2826.14	0.3
	50.0	−10.531	−2.5857	5472.98	822.391	0.3

3.2. Molecular Interaction Simulation Results

Molecular interactions of n-octanol, n-dodecane, and n-tridecane were simulated, as shown in Figure 5. The interaction energies are −32.314 kJ/mol for n-octanol/n-dodecane, −32.629 kJ/mol for n-octanol/n-tridecane, and −25.593 kJ/mol for n-dodecane/n-tridecane. The energy difference (ΔE) is 5.314 kJ/mol for the n-octanol/n-dodecane system, indicating a positive deviation, consistent with the VLE data (maximum activity coefficient ≈ 3.015, Table A4. For n-octanol/n-tridecane, ΔE = 6.231 kJ/mol, also showing a positive deviation, supported by VLE data (maximum activity coefficient ≈ 3.366, Table A5). In contrast, the n-dodecane/n-tridecane system exhibits a small ΔE of 1.091 kJ/mol, suggesting only a slight positive deviation, in agreement with the maximum activity coefficient of approximately 1.018 (Table A6) from VLE measurements.

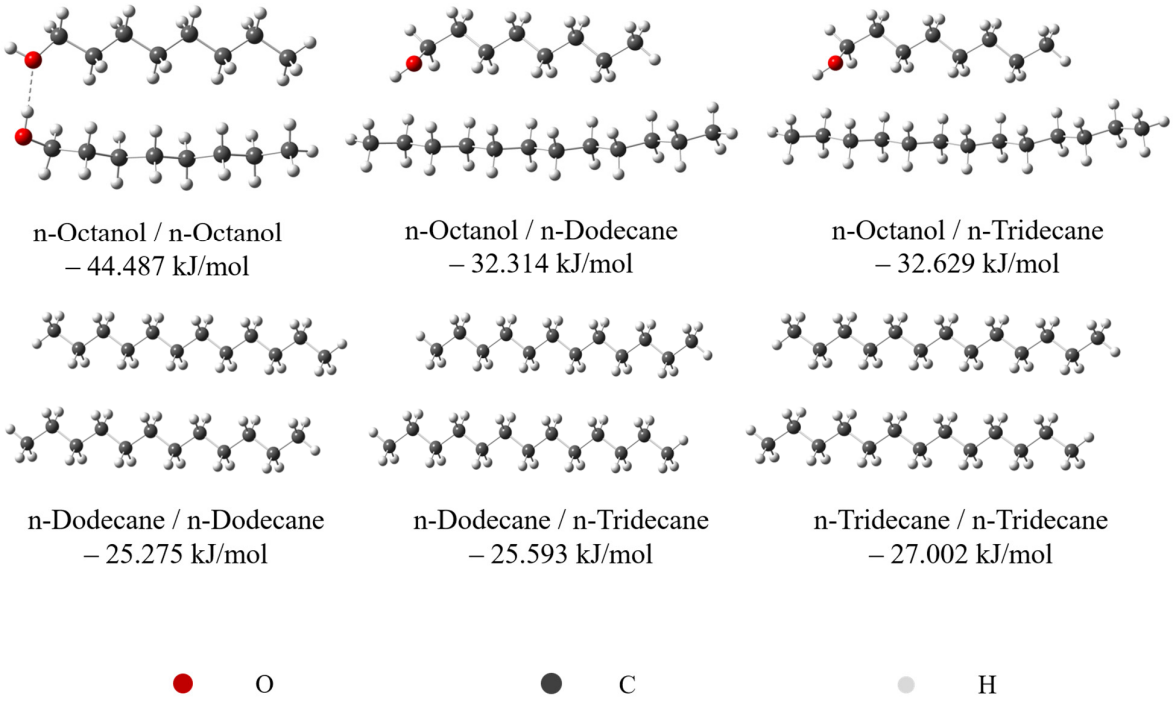

Figure 5. Molecular interaction simulation results for individual components and binary systems.

4. Process Design and Optimization

4.1. HVPSD-5C Process

Based on the analysis of the relative volatility and boiling-point distribution (Tables A1–A6 and A13), a High-Vacuum Pressure-Swing Distillation with Five Columns (HVPSD-5C) Process was designed (Figure 6) with the NRTL thermodynamic model integrated. The base cases were derived from DSTWU shortcut calculations, converged in RADFRAC under mass-balance constraints, and are detailed in Table A14. Sensitivity analyses were performed by varying one parameter at a time from these base case values.

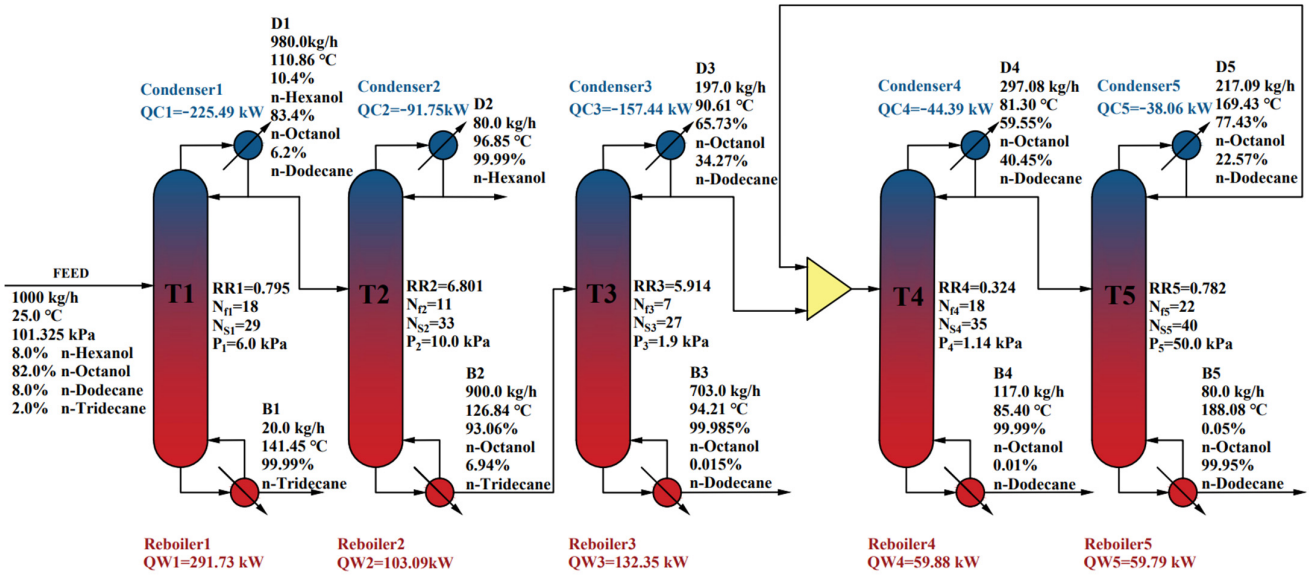

Figure 6. Schematic diagram of the HVPSD-5C process.

In column T1, pure n-tridecane is withdrawn from the bottom, and the overhead distillate is sent to column T2. In column T2, pure n-hexanol is obtained as the distillate, and the bottom mixture of n-octanol and n-dodecane is fed to column T3. The n-octanol/n-dodecane azeotrope distilled from the top of column T3 is mixed with the overhead distillate from column T5, and then fed to the low-pressure column T4. In column T4, pure n-octanol is withdrawn from the bottom, and the overhead azeotrope is sent to the high-pressure column T5. In column T5, pure n-dodecane is withdrawn from the bottom, and the overhead distillate is depressurized and recycled back to column T4. Thus, complete separation of the quaternary mixture is achieved.

To minimize the TAC, the number of theoretical stages, the feed stage location, and the operating pressure of column T1 were optimized. As shown in Figure 7, increasing the operating pressure reduces the column diameter and lowers the costs associated with the vacuum system, but also increases the reboiler duty and corresponding expenses. Increasing the number of theoretical stages significantly raises the capital cost; therefore, reducing the number of stages while still meeting the separation requirements is more economical. Column T1 achieves the minimum TAC at an operating pressure of 6.0 kPa with 29 theoretical stages and a feed stage located at the 18th stage, while satisfying the separation requirements.

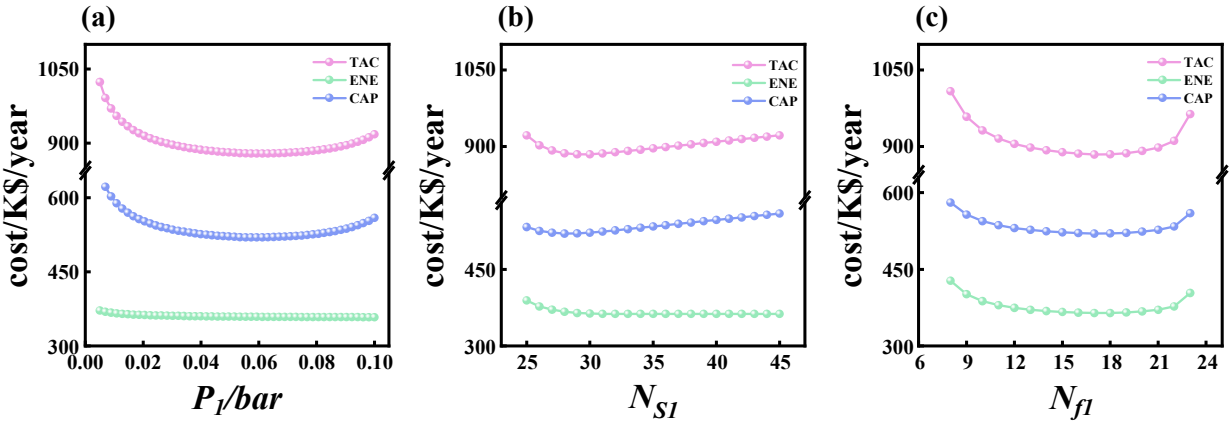

Figure 7. Effects of key parameters on economic indicators. (**a**) The impact of P_1 on energy costs (ENE), capital costs (CAP), and TAC. (**b**) The impact of N_{S1} on energy costs (ENE), capital costs (CAP), and TAC. (**c**) The impact of N_{f1} on energy costs (ENE), capital costs (CAP), and TAC.

The same method was also used to optimize columns T2–T5, and the operating conditions that minimize the total annual cost for each column are shown in Figure 8. For column T2, an operating pressure of 10.0 kPa, a number of theoretical stages of 33, and a feed-stage location of the 11th stage; for column T3, an operating pressure of 1.9 kPa, 27 theoretical stages, and a feed stage at the 7th stage; for column T4, an operating pressure of 1.14 kPa, 35 theoretical stages, and a feed stage at the 18th stage; and for column T5, an operating pressure of 50.0 kPa, 40 theoretical stages, and a feed stage at the 22nd stage. The optimized process has a TAC of 6.18×10^5 \$/year and a CO_2 emission rate of 262.032 kg/h.

4.2. HPI-HVPSD-5C Process

To maximize thermodynamic efficiency, the HPI-HVPSD-5C process incorporates advanced heat-pump distillation (HPD) and cross-column heat integration (HI) strategies (Figure 9). In the heat-pump design, the β parameter defined by Modk and Lang [42] is adopted, and β is fixed at 1, corresponding to the conventional vapor-recompression heat-pump configuration, wherein the working fluid of the compressor originates entirely from the overhead vapor. The feasibility of these configurations was determined by the temperature gradients (Δt) across the columns, which were calculated as T1 (30.59 °C), T2 (34.00 °C), T3 (3.60 °C), T4 (4.40 °C), and T5 (19.07 °C). The process employs three heat integration technologies: the T1–T2 inter-column heat pump utilizes a temperature difference of 16.00 °C, compressing the overhead vapor of T1 to 16.44 kPa to supply 103.09 kW of heat to the bottom of T2; the T3 internal heat pump utilizes a small temperature difference, compressing the overhead vapor to 3.8 kPa to supply 132.34 kW of heat to its own bottom; the T4–T5 heat integration utilizes the pressure difference, providing 44.39 kW of heat from the overhead of T5 to the bottom of T4 via E6, which, although requiring additional heat input, achieves partial heat recovery. In the current process, no superheater is installed before the compressor. Since the inlet steam temperature is already 14 °C and 6.5 °C higher than the dew point, it is sufficient to prevent condensation and no additional superheater is required.

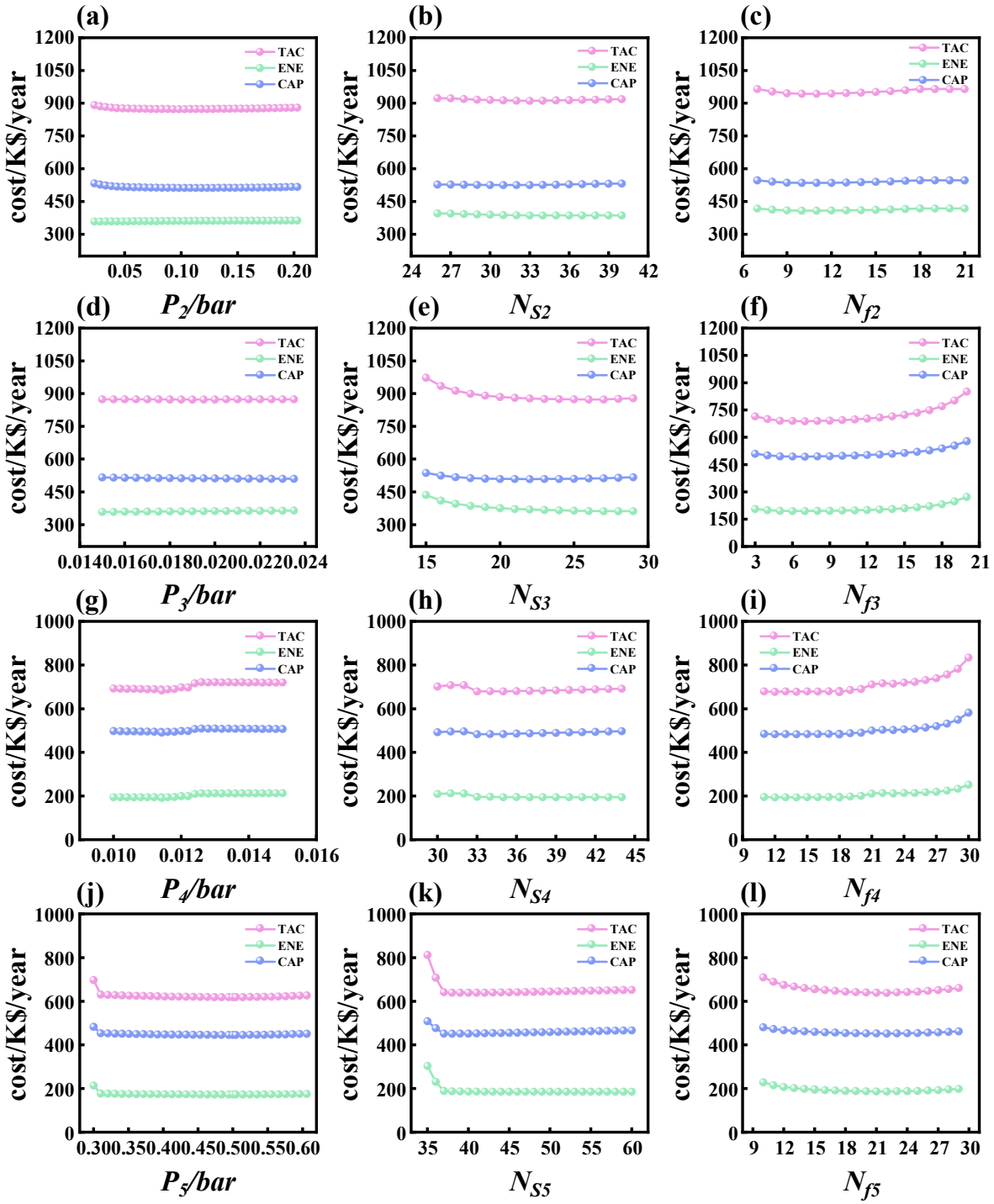

Figure 8. Effects of key parameters on economic indicators (**a**) P_2 on TAC, ENE, and CAP; (**b**) N_{S2} on TAC, ENE, and CAP; (**c**) N_{f2} on TAC, ENE, and CAP; (**d**) P_3 on TAC, ENE, and CAP; (**e**) N_{S3} on TAC, ENE, and CAP; (**f**) N_{f3} on TAC, ENE, and CAP; (**g**) P_4 on TAC, ENE, and CAP; (**h**) N_{S4} on TAC, ENE, and CAP; (**i**) N_{f4} on TAC, ENE, and CAP; (**j**) P_5 on TAC, ENE, and CAP; (**k**) N_{S5} on TAC, ENE, and CAP; (**l**) N_{f5} on TAC, ENE, and CAP.

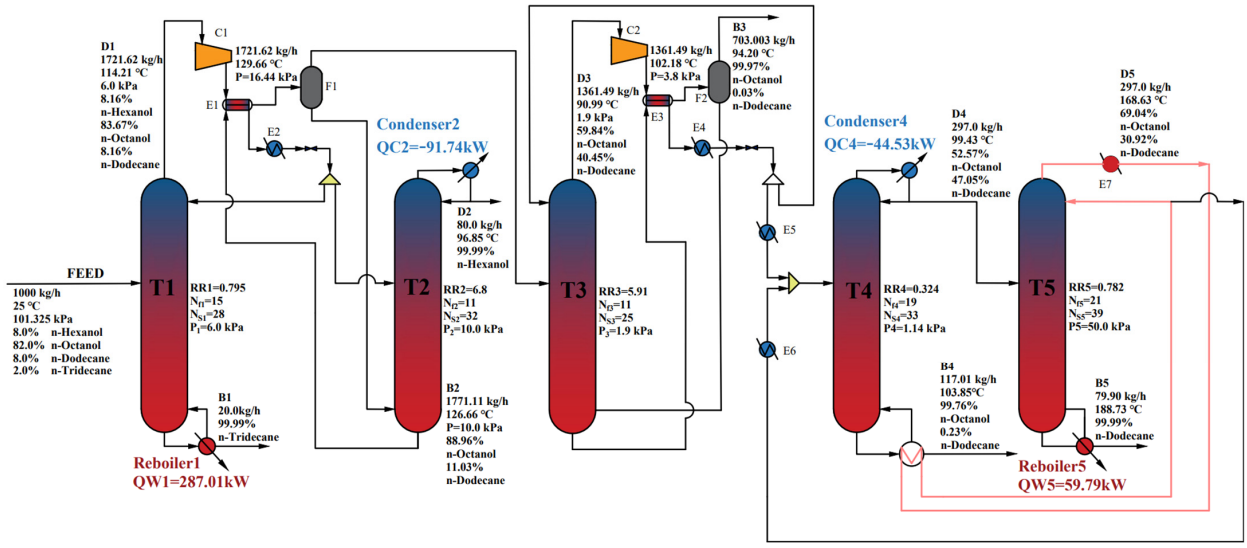

Figure 9. Schematic diagram of the HPI-HVPSD-5C process.

In the HPI-HVPSD-5C process, the performance of the heat-pump system is primarily governed by the compressor's compression ratio. Through sensitivity analysis, using the net benefit between heat-transfer capacity and compressor-power consumption as the evaluation metric, the relationships among compressor exit temperature, heat-transfer rate, and compression ratio are elucidated (Figure 10). By comprehensively balancing the increase in heat-transfer rate against the rise in energy consumption, the optimal compression ratio is determined to be 2.74, at which the system achieves the best trade-off between heat-transfer demand and energy consumption. The optimal compression ratio for the other compressor is 2.00 (Figure A1).

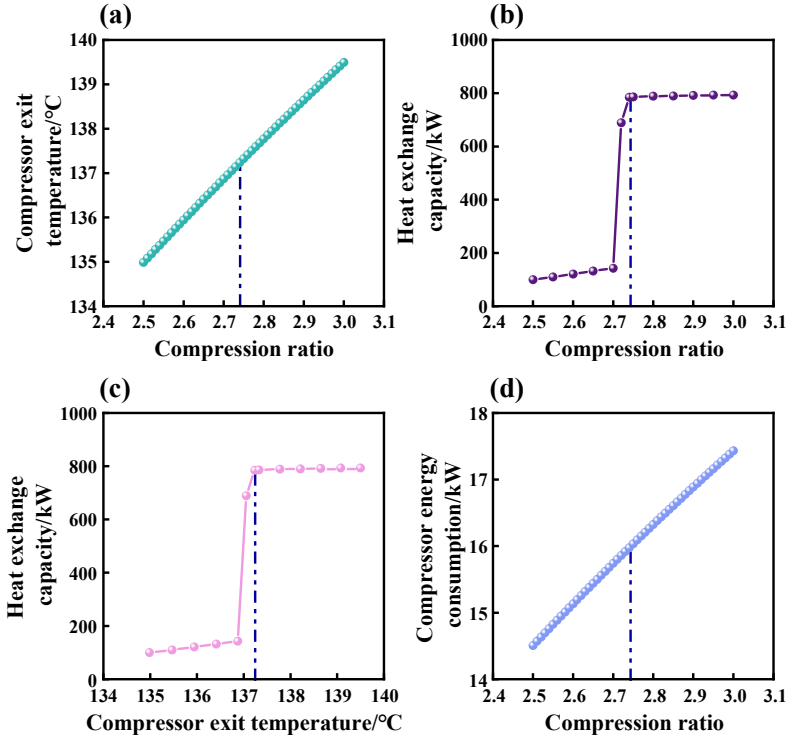

Figure 10. Sensitivity analysis of compressor 1. (**a**) Compression ratio versus compressor exit temperature. (**b**) Compression ratio versus heat-exchange capacity. (**c**) Compressor exit temperature versus heat-exchange capacity. (**d**) Compression ratio versus compressor energy consumption.

Figure 11 displays the Temperature–Enthalpy (T–H) diagram obtained from pinch analysis. This diagram illustrates the heat-integration potential of the overall process. The Hot Composite Curve (HCC) and Cold Composite Curve (CCC) represent the process hot-utility (heat sink) requirements and cold-utility (heat source) requirements, respectively. The shaded area between the curves indicates the net recoverable heat exchange potential. Ultimately, the TAC for the HPI-HVPSD-5C process is 5.10×10^5 \$/year, and the CO_2 emissions are 219.868 kg/h.

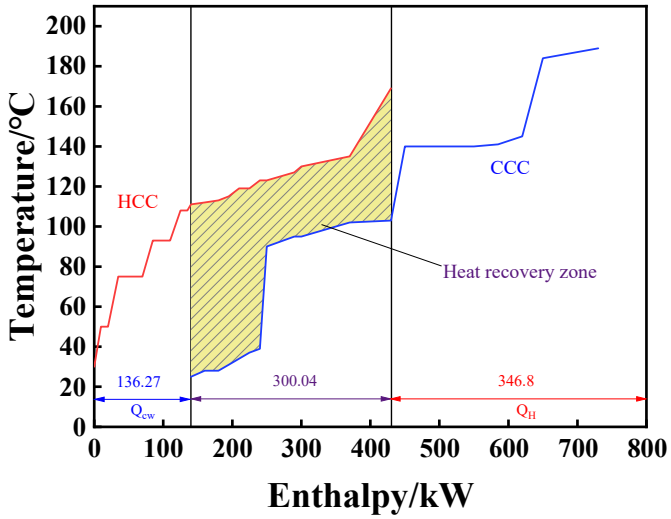

Figure 11. Temperature–Enthalpy diagram.

5. Process Comparison Process Evaluation

5.1. Economic Assessment

The HPI-HVPSD-5C process yields a 17.48% reduction in TAC compared to the conventional HVPSD-5C (Figure 12), decreasing from 6.18×10^5 \$/year to 5.10×10^5 \$/year.

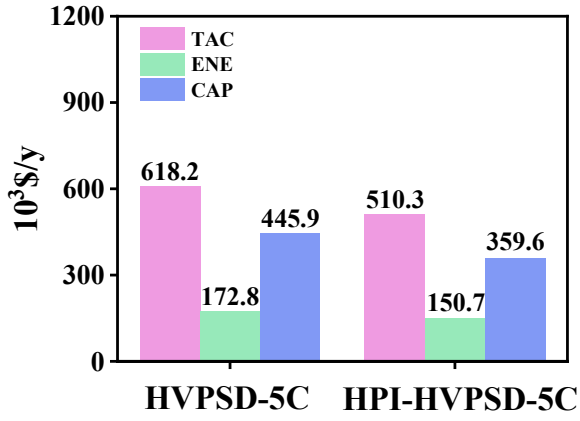

Figure 12. TAC comparison: HVPSD-5C versus HPI-HVPSD-5C.

5.2. Environmental Assessment

As shown in Figure 13, compared with the HVPSC-5C process, the HPI-HVPSD-5C process achieves CO_2 emissions of 219.868 kg/h and energy consumption of 346.80 kW, representing reductions of 16.09% and 46.39%, respectively. This improvement is mainly attributed to the recovery and utilization of waste heat, thereby reducing the demand for steam and cooling water.

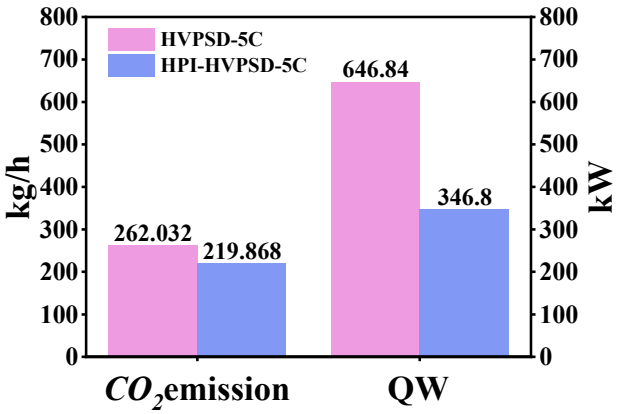

Figure 13. CO_2 emissions and energy consumption: HVPSD-5C versus HPI-HVPSD-5C.

6. Conclusions

This study investigates the separation of alcohol/alkane azeotropic mixtures from fatty alcohol production via high-pressure oil hydrogenation. VLE data for n-hexanol, n-octanol, n-dodecane, and n-tridecane were experimentally established, regressed using NRTL, UNIQUAC, and Wilson, and validated using molecular binding energy calculations. Pressure's impact on separation was studied, enabling the design and optimization of HVPSD-5C and HPI-HVPSD-5C processes. A rigorous sequential iterative optimization approach was applied to tune the operating parameters of each column, aiming to minimize the TAC. Compared to HVPSD-5C, the integrated HPI-HVPSD-5C process, which incorporates heat pump and heat integration, demonstrated significant improvements in overall performance, achieving a 17.48% reduction in TAC, a 16.09% decrease in CO_2 emissions, and a 12.79% reduction in energy consumption cost. This study proposes a novel, efficient, and low-carbon separation process for alcohol/alkane azeotropes and provides theoretical and practical guidance for pressure-sensitive azeotropic systems.

Author Contributions: C.L.: Funding acquisition, methodology, supervision; T.M.: data curation, writing—original draft, investigation; Y.S.: writing—review and editing, conceptualization; K.S.: data curation, writing—review and editing; W.L.: data curation, methodology; R.W.: data curation, methodology, writing—review and editing; J.L.: writing—review and editing, project administration. All authors have read and agreed to the published version of the manuscript.

Funding: National Natural Science Foundation of China (Nos. 22408082, 22508307), the China Postdoctoral Science Foundation (Grant 2023M740969), and the Scientific Research Project of Tianjin Education Commission (Grant 2023KJ293, 2021KJ113).

Data Availability Statement: This article includes the original contributions proposed in this study. For any further inquiries, please contact the corresponding author.

Acknowledgments: Funding for this research was received from the National Natural Science Foundation of China (Nos. 22408082, 22508307), the China Postdoctoral Science Foundation (Grant 2023M740969), and the Scientific Research Project of Tianjin Education Commission (Grant 2023KJ293, 2021KJ113).

Conflicts of Interest: The authors declare no conflicts of interest.

Appendix A

Table A1. VLE experimental data for n-hexanol/n-octanol binary system at 1.0 kPa (equilibrium temperature—T; liquid-phase molar fraction—x_i; gas-phase molar fraction—y_i; activity coefficient—γ_i; and relative volatility—α_{12}).

	T/K	x_1	x_2	y_1	y_2	γ_1	γ_2	α_{12}
1.0 kPa	360.2	0.0000	1.0000	0.0000	1.0000			
	356.15	0.0277	0.9583	0.2113	0.8017	1.5316	0.8464	9.1114
	352.55	0.0555	0.9305	0.3269	0.6861	1.4367	0.9314	7.9876
	347.95	0.1613	0.8247	0.5382	0.4748	1.0515	0.9747	5.7960
	346.05	0.2060	0.7800	0.6298	0.3832	1.0741	0.9415	6.2251
	343.45	0.2867	0.6993	0.7147	0.2983	1.0186	0.9718	5.8449
	342.15	0.3507	0.6353	0.7678	0.2452	0.9659	0.9599	5.6728
	339.85	0.4262	0.5598	0.8124	0.2006	0.9650	1.0433	5.3185
	338.45	0.4947	0.4913	0.8452	0.1678	0.9417	1.0961	5.0004
	337.65	0.5410	0.4450	0.8851	0.1279	0.9472	0.9755	5.6909
	336.05	0.6056	0.3804	0.8973	0.1157	0.9472	1.1558	4.8715
	334.65	0.6527	0.3333	0.9175	0.0955	0.9810	1.2041	4.9038
	334.05	0.6994	0.2866	0.9377	0.0753	0.9718	1.1523	5.1036
	333.55	0.7361	0.2499	0.9503	0.0627	0.9660	1.1412	5.1454
	332.25	0.7793	0.2067	0.9627	0.0503	1.0045	1.2159	5.0816
	331.55	0.8199	0.1661	0.9743	0.0387	1.0108	1.2262	5.1030
	331.45	0.8608	0.1252	0.9832	0.0298	0.9779	1.2604	4.8074
	330.35	0.9021	0.0839	0.9912	0.0218	1.0104	1.4940	4.2331
	328.35	0.9390	0.0470	0.9989	0.0141	1.1159	2.0085	3.5430
	328.1	1.0000	0.0000	1.0000	0.0000			

Standard uncertainties u of T, p, x and y are u (T) = 1 K, u (p) = 1.0 kPa, u (x) = 0.005, and u (y) = 0.005.

Table A2. VLE experimental data for n-hexanol/n-dodecane binary system at 1.0 kPa (equilibrium temperature—T; liquid-phase molar fraction—x_i; gas-phase molar fraction—y_i; activity coefficient γ_i; and relative volatility—α_{12}).

	T/K	x_1	x_2	y_1	y_2	γ_1	γ_2	α_{12}
1.0 kPa	361.15	0.0000	1.0000	0.0000	1.0000			
	351.15	0.0158	0.9842	0.3572	0.6428	5.9536	0.9899	34.5972
	340.15	0.0682	0.9318	0.6458	0.3542	4.7111	1.0849	24.9265
	336.65	0.1326	0.8674	0.7319	0.2681	3.3987	1.0910	17.8545
	334.75	0.2226	0.7774	0.7974	0.2026	2.4838	1.0351	13.7391
	333.75	0.3115	0.6885	0.8215	0.1785	1.9486	1.0961	10.1730
	333.25	0.3729	0.6271	0.8269	0.1731	1.6914	1.2043	8.0338
	332.95	0.4325	0.5675	0.8284	0.1716	1.4889	1.3445	6.3339
	332.75	0.4611	0.5389	0.8290	0.1710	1.4156	1.4292	5.6642
	332.25	0.5163	0.4837	0.8383	0.1617	1.3201	1.5541	4.8561
	331.95	0.5506	0.4494	0.8463	0.1537	1.2742	1.6200	4.4954
	331.75	0.6070	0.3930	0.8585	0.1415	1.1875	1.7281	3.9270
	331.65	0.6726	0.3274	0.8711	0.1289	1.0945	1.9021	3.2881
	331.25	0.7160	0.2840	0.8799	0.1201	1.0658	2.0957	2.9052
	331.15	0.7483	0.2517	0.8903	0.1097	1.0386	2.1731	2.7302
	331.05	0.8054	0.1946	0.9069	0.0931	0.9893	2.4017	2.3529
	330.75	0.8405	0.1595	0.9164	0.0836	0.9768	2.6826	2.0795
	330.65	0.8993	0.1007	0.9330	0.0670	0.9355	3.4288	1.5580
	330.45	0.9379	0.0621	0.9535	0.0465	0.9288	3.9083	1.3568
	330.25	0.9942	0.0058	0.9943	0.0057	0.9256	5.2450	1.0075
	330.20	1.0000	0.0000	1.0000	0.0000			

Standard uncertainties u of T, p, x and y are u (T) = 1 K, u (p) = 1.0 kPa, u (x) = 0.005, and u (y) = 0.005.

Table A3. VLE experimental data for n-hexanol/n-tridecane binary system at 1.0 kPa (equilibrium temperature—T; liquid-phase molar fraction—x_i; gas-phase molar fraction—y_i; activity coefficient—γ_i; and relative volatility—α_{12}).

	T/K	x_1	x_2	y_1	y_2	γ_1	γ_2	α_{12}
1.0 kPa	374.3	0.0000	1.0000	0.0000	1.0000			
	361.3	0.1013	0.8987	0.6020	0.3980	0.9127	0.8863	13.4121
	357.75	0.1939	0.8061	0.7657	0.2343	0.7291	0.7074	13.5854
	353.05	0.2789	0.7211	0.8428	0.1572	0.7173	0.6963	13.8638
	349.35	0.3571	0.6429	0.8866	0.1134	0.7231	0.7028	14.0736
	346.4	0.4292	0.5708	0.9146	0.0854	0.7335	0.7137	14.2448
	343.85	0.4961	0.5039	0.9339	0.0661	0.7514	0.7331	14.3648
	341.7	0.5582	0.4418	0.9481	0.0519	0.7695	0.7530	14.4600
	339.85	0.6160	0.3840	0.9578	0.0422	0.7871	0.7941	14.1389
	338.15	0.6700	0.3300	0.9668	0.0332	0.8102	0.8109	14.3586
	336.65	0.7205	0.2795	0.9731	0.0269	0.8318	0.8571	14.0389
	335.3	0.7680	0.2320	0.9794	0.0206	0.8544	0.8661	14.3551
	334.05	0.8125	0.1875	0.9841	0.0159	0.8780	0.9013	14.2535
	332.9	0.8544	0.1456	0.9881	0.0119	0.9020	0.9382	14.1384
	331.85	0.8939	0.1061	0.9918	0.0082	0.9257	0.9520	14.3659
	330.8	0.9312	0.0688	0.9948	0.0052	0.9540	0.9973	14.1971
	329.95	0.9665	0.0335	0.9976	0.0024	0.9742	1.0267	14.1360
	329.05	1.0000	0.0000	1.0000	0.0000			

Standard uncertainties u of T, p, x and y are u (T) = 1 K, u (p) = 1.0 kPa, u (x) = 0.005, and u (y) = 0.005.

Table A4. VLE experimental data for n-octanol/n-dodecane binary system at 1.0 and 50.0 kPa (equilibrium temperature—T; liquid-phase molar fraction—x_i; gas-phase molar fraction—y_i; activity coefficient—γ_i; and relative volatility—α_{12}).

	T/K	x_1	x_2	y_1	y_2	γ_1	γ_2	α_{12}
1.0 kPa	358.62	1.0000	0.0000	1.0000	0.0000			
	356.85	0.8741	0.1259	0.7472	0.2528	0.9516	1.9463	0.4259
	355.65	0.8462	0.1538	0.6853	0.3147	0.9609	2.1346	0.3957
	354.25	0.8129	0.1871	0.6519	0.3481	1.0261	2.1141	0.4312
	353.65	0.8074	0.1953	0.6409	0.3591	1.0525	2.1694	0.4330
	352.15	0.7189	0.2811	0.5764	0.4236	1.1501	1.9516	0.5321
	351.25	0.6500	0.3500	0.5694	0.4306	1.3203	1.6864	0.7121
	350.05	0.5749	0.4251	0.5535	0.4465	1.5509	1.5537	0.9165
	351.05	0.4902	0.5098	0.5064	0.4936	1.5743	1.3441	1.0670
	351.55	0.4329	0.5671	0.4868	0.5132	1.6670	1.2172	1.2425
	351.65	0.4269	0.5731	0.4821	0.5179	1.6652	1.2077	1.2500
	351.65	0.3990	0.6010	0.4781	0.5219	1.7664	1.1608	1.3796
	352.05	0.3659	0.6341	0.4715	0.5285	1.8583	1.0864	1.5459
	352.05	0.2926	0.7074	0.4241	0.5759	2.0909	1.0610	1.7810
	352.55	0.2404	0.7596	0.3702	0.6298	2.1606	1.0474	1.8569
	352.65	0.2269	0.7731	0.3560	0.6440	2.1897	1.0457	1.8835
	352.75	0.1940	0.8060	0.3252	0.6748	2.3269	1.0444	2.0024
	353.55	0.1660	0.8340	0.2849	0.7151	2.2803	1.0177	2.0013
	354.65	0.0709	0.9291	0.1523	0.8477	2.6885	1.0117	2.3534
	354.75	0.0610	0.9390	0.1351	0.8649	2.7603	1.0151	2.4065
	355.45	0.0454	0.9546	0.1041	0.8959	2.7530	0.9908	2.6771
	355.65	0.0320	0.9680	0.0814	0.9186	3.0148	0.9898	2.6771
	355.85	0.0000	1.0000	0.0000	1.0000			
50.0 kPa	467.85	1.0000	0.0000	1.0000	0.0000			

Table A4. *Cont.*

	T/K	x_1	x_2	y_1	y_2	γ_1	γ_2	α_{12}
	460.75	0.8814	0.1286	0.7703	0.2197	0.9015	1.0096	4.0163
	453.25	0.8272	0.1828	0.6616	0.3284	1.0193	1.3274	3.2321
	451.15	0.7915	0.2185	0.5958	0.3942	1.0196	1.3274	3.2321
	448.95	0.7331	0.2769	0.5139	0.4761	1.0127	1.4508	2.1364
	447.35	0.6811	0.3289	0.4627	0.5273	1.0290	1.4228	1.8331
	445.95	0.5824	0.4276	0.3943	0.5957	1.0693	1.2926	1.4690
	445.35	0.5479	0.4621	0.3758	0.6142	1.1030	1.2572	1.4038
	445.05	0.5220	0.4880	0.3580	0.6547	1.1129	1.2368	1.3422
	444.65	0.4748	0.5352	0.3353	0.6547	1.1600	1.1834	1.2766
	444.25	0.4084	0.6016	0.3032	0.6868	1.2340	1.1189	1.2092
	444.15	0.3786	0.6314	0.2879	0.7021	1.2679	1.0933	1.1839
	443.85	0.3362	0.6738	0.2672	0.7228	1.3373	1.0650	1.1709
	443.75	0.3065	0.7035	0.2515	0.7385	1.3850	1.0456	1.1616
	443.65	0.2893	0.7207	0.2389	0.7511	1.3981	1.0414	1.1450
	443.45	0.2424	0.7676	0.2119	0.7781	1.4891	1.0195	1.1455
	442.45	0.2029	0.8071	0.1845	0.8055	2.0518	1.3572	1.5325
	442.45	0.1631	0.8469	0.1542	0.8358	1.6604	1.0255	1.1601
	443.45	0.1358	0.8742	0.1291	0.8609	1.6200	0.9904	1.0941
	443.55	0.1110	0.8990	0.1091	0.8809	1.6681	0.9824	1.0954
	443.75	0.0657	0.9393	0.0763	0.9237	1.9602	0.9795	1.2315
	443.85	0.0487	0.9563	0.0573	0.9427	1.9784	0.9787	1.2206
	444.05	0.0277	0.9743	0.0334	0.9666	2.0164	0.9786	1.2206
	444.65	0.0000	1.0000	0.0000	1.0000			

Standard uncertainties u of T, p, x and y are u (T) = 1 K, u (p) = 1.0 kPa, u (x) = 0.005, and u (y) = 0.005.

Table A5. LE experimental data for n-octanol/n-tridecane binary system at 1.0 and 50.0 kPa (equilibrium temperature—T; liquid-phase molar fraction—x_i; gas-phase molar fraction—y_i; activity coefficient—γ_i; and relative volatility—α_{12}).

	T/K	x_1	x_2	y_1	y_2	γ_1	γ_2	α_{12}
1.0 kPa	373.75	0.0000	1.0000	0.0000	1.0000			
	369.95	0.0475	0.9465	0.2917	0.7143	2.8013	0.9479	8.1387
	363.65	0.0825	0.9115	0.4275	0.5785	3.3662	1.1158	8.1686
	360.65	0.1422	0.8518	0.5333	0.4727	2.8980	1.1515	6.7546
	359.05	0.2488	0.7452	0.6174	0.3886	2.1090	1.1833	4.7602
	357.95	0.3289	0.6651	0.6594	0.3466	1.8193	1.2588	3.8469
	357.65	0.4199	0.5741	0.6841	0.3219	1.5053	1.3776	2.9055
	357.55	0.4739	0.5201	0.6925	0.3135	1.3582	1.4894	2.4243
	356.95	0.5322	0.4618	0.7120	0.2940	1.2893	1.6279	2.1015
	356.75	0.5722	0.4218	0.7218	0.2842	1.2304	1.7432	1.8715
	356.65	0.6358	0.3582	0.7454	0.2606	1.1505	1.8928	1.6112
	356.25	0.7081	0.2859	0.7800	0.2260	1.1076	2.1042	1.3935
	355.85	0.7434	0.2506	0.8002	0.2058	1.1090	2.2373	1.3105
	355.15	0.8077	0.1863	0.8263	0.1797	1.1001	2.7361	1.0605
	356.45	0.8494	0.1446	0.8543	0.1517	0.9992	2.7600	0.9589
	356.55	0.8862	0.1078	0.8854	0.1206	0.9866	2.9254	0.8936
	356.85	0.9238	0.0702	0.9140	0.0920	0.9593	3.3703	0.7550
	356.85	0.9873	0.0067	0.9912	0.0148	0.9735	5.6506	0.4570
	357.65	1.0000	0.0000	1.0000	0.0000			
50.0 kPa	481.15	0.0000	1.0000	0.0000	1.0000			
	474.95	0.0536	0.9464	0.1851	0.9464	1.3767	0.9921	4.0116
	466.85	0.1077	0.8923	0.3490	0.8923	1.6106	1.0561	4.4439
	461.85	0.1684	0.8316	0.4735	0.8316	1.6097	1.0605	4.4411
	451.95	0.4069	0.5931	0.7009	0.5931	1.3241	1.1416	3.4156

Table A5. *Cont.*

	T/K	x_1	x_2	y_1	y_2	γ_1	γ_2	α_{12}
	458.15	0.2375	0.7625	0.5654	0.7625	1.5186	1.0663	4.1781
	454.15	0.3745	0.6255	0.6817	0.6255	1.3086	1.0757	3.5783
	450.15	0.5061	0.4939	0.7498	0.4939	1.2041	1.2137	2.9244
	449.15	0.5620	0.4380	0.7701	0.4380	1.1491	1.2977	2.6113
	448.45	0.5850	0.4150	0.7800	0.4150	1.1429	1.3402	2.5157
	447.65	0.6378	0.3622	0.7998	0.3622	1.1023	1.4338	2.2688
	447.15	0.7222	0.2778	0.8515	0.2778	1.0530	1.4086	2.2066
	446.75	0.7601	0.2399	0.8721	0.2399	1.0378	1.4232	2.1528
	446.35	0.7948	0.2052	0.8869	0.2052	1.0222	1.4905	2.0251
	445.95	0.8284	0.1716	0.8992	0.1716	1.0072	1.6093	1.8482
	445.45	0.8817	0.1183	0.9252	0.1183	0.9894	1.7601	1.6603
	444.85	0.9272	0.0728	0.9530	0.0728	0.9879	1.8343	1.5911
	444.35	0.9834	0.0166	0.9886	0.0166	0.9820	1.9770	1.4677
	444.05	1.0000	0.0000	1.0000	0.0000			

Standard uncertainties u of T, p, x and y are u (T) = 1 K, u (p) = 1.0 kPa, u (x) = 0.005, and u (y) = 0.005.

Table A6. VLE experimental data of n-dodecane/n-tridecane binary system at 1.0 and 50.0 kPa (equilibrium temperature—T; liquid-phase molar fraction—x_i; gas-phase molar fraction—y_i; activity coefficient—γ_i; and relative volatility—α_{12}).

	T/K	x_1	x_2	y_1	y_2	γ_1	γ_2	α_{12}
1.0 kPa	374.25	0.0000	1.0000	0.0000	1.0000			
	373.15	0.0419	0.9581	0.0772	0.9228	0.0016	0.9412	1.9135
	371.15	0.1026	0.8974	0.1929	0.8071	0.0104	0.8242	2.0896
	370.85	0.1732	0.8268	0.3020	0.6980	0.0287	0.6916	2.0656
	369.55	0.2328	0.7672	0.3858	0.6142	0.0525	0.6044	2.0700
	368.65	0.2941	0.7059	0.4681	0.5319	0.0841	0.5049	2.1125
	368.15	0.3589	0.6411	0.5455	0.4545	0.1225	0.4023	2.1442
	366.45	0.4232	0.5768	0.6035	0.3965	0.1738	0.3457	2.0749
	365.55	0.4939	0.5061	0.6792	0.3208	0.2387	0.2575	2.1688
	364.75	0.5459	0.4541	0.7249	0.2751	0.2931	0.2069	2.1925
	363.25	0.6179	0.3821	0.7788	0.2212	0.3845	0.1519	2.1770
	363.15	0.6875	0.3125	0.8198	0.1802	0.4526	0.1018	2.0668
	361.95	0.7563	0.2437	0.8662	0.1338	0.5591	0.0630	2.0855
	361.45	0.8026	0.1974	0.8936	0.1064	0.6280	0.0417	2.0668
	361.15	0.8556	0.1444	0.9289	0.0711	0.7068	0.0207	2.2048
	359.65	0.9266	0.0734	0.9644	0.0356	0.8587	0.0057	2.1481
	359.35	0.9735	0.0265	0.9878	0.0122	0.9387	0.0007	2.2076
	359.15	1.0000	0.0000	1.0000	0.0000			
50.0 kPa	480.75	0.0000	1.0000	0.0000	1.0000			
	479.85	0.0615	0.9435	0.0852	0.9435	0.8645	0.9724	1.4352
	478.65	0.1218	0.8832	0.1750	0.8832	0.9247	0.9670	1.5474
	477.35	0.1899	0.8151	0.2686	0.8151	0.9408	0.9615	1.5873
	476.35	0.2527	0.7523	0.3539	0.7523	0.9554	0.9448	1.6434
	475.15	0.3126	0.6924	0.4250	0.6924	0.9564	0.9432	1.6518
	473.45	0.3920	0.6130	0.5404	0.6130	1.0130	0.8908	1.8588
	470.25	0.4602	0.5448	0.5938	0.5448	1.0306	0.9674	1.7525
	469.05	0.5307	0.4743	0.6488	0.4743	1.0077	0.9922	1.6747
	467.95	0.5983	0.4067	0.7061	0.4067	1.0017	0.9963	1.6616
	467.05	0.6438	0.3612	0.7433	0.3612	1.0036	1.0031	1.6566
	466.35	0.6991	0.3059	0.7866	0.3059	0.9965	1.0006	1.6514
	465.35	0.7512	0.2538	0.8241	0.2538	0.9982	1.0179	1.6294
	464.35	0.8083	0.1967	0.8690	0.1967	1.0049	0.9973	1.6778
	463.15	0.8838	0.1212	0.9194	0.1212	1.0046	1.0059	1.6672
	461.85	0.9648	0.0402	0.9704	0.0402	1.0065	1.0257	1.6426
	461.65	1.0000	0.0000	1.0000	0.0000			

Standard uncertainties u of T, p, x and y are u (T) = 1 K, u (p) = 1.0 kPa, u (x) = 0.005, and u (y) = 0.005.

Table A7. Analytical conditions used in GC.

Items	Description
Detector	Hydrogen flame detector (FID)
Column	Inert Cap FFAP (0.25 μm × 0.25 mm × 30 m)
Carrier gas and flow rate	H_2, 20 mL/min
Vaporizer temperature	513.15 K
Detector temperature	523.15 K
Temperature program	The program temperature was set to 453.15 K, and the sample analysis time was 4 min.

Table A8. Economic basis.

Category	Formula	Unit
Columns		
Diameter (D)	Aspen tray sizing	m
Length (L)	$1.2 \times 0.6096 \times (N_t - 2)$ 0.6096 refers to the tray spacing	m
Column shell cost (ShellC)	$M\&S/280 \times 937.636 \times D^{1.066} \times L^{0.802} \times (2.18 + F_c)$	$
Correction factors	$F_c = F_p \cdot F_m = 1 \times 3.67 = 3.67$	
Plate capital cost (PlateC)	$M\&S/280 \times 97.243 \times D^{1.55} \times L \times F_c$	$
Correction factors	$F_c = F_s + F_t + F_m = 1 + 0 + 1.7 = 2.7$	
Compressor	$M\&S/280 \times 517.5 \times (bhp)^{0.82} \times (2.11 + F_c)$	$
Correction factors	$F_c = F_d = 1$	
Installation cost (InstC)	$(C_{shell} + C_{trays}) \times (M\&S/1440) \times 3.05$	$
Reboiler exchanger area (A_R)	0.568	kW/K·m^2
Condensers exchanger area (A_C)	0.852	kW/K·m^2
Heat exchanger area (A_H)	$A_H = Q_H/(U_H \times \Delta T_{In})$ Heat exchanger coefficient (UH): Liquid–liquid: 0.57 Liquid–vapor: 0.20 Vapor–vaporizing liquid: 0.28 Vapor–vapor: 0.17 Condensing vapor–vaporizing liquid: 1.2	kW/K·m^2
Heat exchanger cost (HEC)	$HEC = 9445.2 \times (A_R^{0.65} + A_C^{0.65} + A_H^{0.65})$	$
Compressor cost (CompC)	$M\&S/280 \times 517.5 \times (bhp)^{0.82} \times (2.11 + F_c)$	$
Correction factors	$F_c = F_d = 1$	
Capital investment	FCI = ShellC + PlateC + HEC + CompC + InstC	$
Energy cost (EC)	$EC = (SC \times Q_R + 0.28 \times Q_C) \times 8000$ Where one year is assumed as 8000 working hour, unit of Q_R and Q_C: GJ/h SC represents the cost of LP, HP steam cooling water = 0.354 $/GJ LP steam (433 K,0.5 MPa) = 7.78 $/GJ HP steam (527 K,1.5 MPa) = 9.88 $/GJ	$/year
Vacuum system		
Flow rate of air leakage	$5 + [0.0298 + 0.03088(\ln P) - 0.0005733(\ln P)^2]V^{0.66}$ Where P is the absolute operating pressure in torr; V is the vessel volume in ft^3.	lb/h
(1) Steam-jet elector		
Size factor (S)	Flow rate (lb/hr)/suction pressure (torr)	
Range of S	0.1–100	
Cost multiplying factor (CM)	One-stage: 1.0, two-stages: 1.8, three-stages: 2.1	
Capital cost	$1690(CM)S^{0.41}$	$
Operating cost	(Steam consumption) × (LP steam cost), the estimated steam consumption is 10 times of the flow rate.	$
(2) Liquid-ring pump		
Size factor (S)	Flow at suction, ft^3/min	
Range of S	50–350	
Capital cost	$6500 \times 1690/1330 \times S^{0.35}$	$
Operating cost	Electricity cost	$
Electricity cost (ElectricityC)	$ElectricityC = 0.5 \times Q_P \times 8000/7$	$/year
Operating cost (OC)	OC = EC + ElectricityC	$/year
TAC	TAC = FCI/payback + OC	$/year
Payback	5-year	
Marshall & Swift index	$M\&S$ = 1638.2 (in 2018)	

Table A9. Parameters of the Antoine equation.

Component	C_{1i}	C_{2i}	C_{3i}	C_{4i}	C_{5i}	C_{6i}	C_{7i}	T_{min}/K	T_{max}/K
n-hexanol	128.512	−12,288	0	0	−15.732	1.2701×10^{-17}	6	228.55	611.3
n-octanol	137.202	−13,667	0	0	−16.826	9.3666×10^{-18}	6	257.65	652.3
n-dodecane	130.562	−11,976	0	0	−16.698	8.0906×10^{-6}	2	263.57	658.0
n-tridecane	130.542	−12,549	0	0	−16.543	7.1275×10^{-6}	2	267.76	675.0

Table A10. Thermodynamic conformance testing using the Herington area method.

I	$\int_{x_1=0}^{x_1=1} \ln\left(\frac{\gamma_1}{\gamma_2}\right) dx_1$
Σ	$\int_{x_1=0}^{x_1=1} \left\|\ln\left(\frac{\gamma_1}{\gamma_2}\right)\right\| dx_1$
D	$\frac{100\|I\|}{\Sigma}$
J	$\frac{150(T_{max}-T_{min})}{T_{min}}$

Table A11. RMSD and AAD values of the quaternary mixture.

System	P/kPa	Model	RMSD (T_1/K)	RMSD (y_1)	AAD (T_1/K)	AAD (y_1)
n-hexanol/n-octanol	1.0	NRTL	1.0564	0.0094	0.0119	0.0081
		UNIQUAC	1.2752	0.0095	0.0165	0.0112
		Wilson	1.4889	0.0442	0.0158	0.0115
n-hexanol/n-dodecane	1.0	NRTL	0.8390	0.0049	0.0133	0.0053
		UNIQUAC	0.8402	0.0060	0.0135	0.0073
		Wilson	0.8422	0.0062	0.0130	0.0057
n-hexanol/n-tridecane	1.0	NRTL	2.3476	0.0379	0.0303	0.0097
		UNIQUAC	2.3432	0.0385	0.0301	0.0106
		Wilson	2.3574	0.0381	0.0303	0.0102
n-octanol/n-dodecane	1.0	NRTL	0.7890	0.0247	0.0065	0.0047
		UNIQUAC	0.7186	0.0227	0.0048	0.0057
		Wilson	0.7057	0.0249	0.0057	0.0085
n-octanol/n-dodecane	50.0	NRTL	1.7290	0.0087	0.0061	0.0094
		UNIQUAC	1.7350	0.0085	0.0063	0.0116
		Wilson	1.7180	0.0104	0.0062	0.0138
n-octanol/n-tridecane	1.0	NRTL	0.5764	0.0106	0.0075	0.0087
		UNIQUAC	0.5844	0.0146	0.0054	0.0114
		Wilson	0.7347	0.0098	0.0074	0.0107
n-octanol/n-tridecane	50.0	NRTL	0.6621	0.0091	0.0032	0.0063
		UNIQUAC	0.6791	0.0084	0.0031	0.0145
		Wilson	1.7533	0.2162	0.0862	0.3897
n-dodecane/n-tridecane	1.0	NRTL	0.3345	0.0040	0.0030	0.0079
		UNIQUAC	0.3363	0.0040	0.0030	0.0081
		Wilson	0.3433	0.0040	0.0030	0.0081
n-dodecane/n-tridecane	50.0	NRTL	0.3714	0.0108	0.0017	0.0056
		UNIQUAC	0.3896	0.0108	0.0018	0.0066
		Wilson	0.3775	0.0114	0.0017	0.0057

Table A12. Calculation formulas for RMSD and AAD values.

RMSD (T_i)	$(\sum_{i=1}^{N} \frac{\left(T_i^{EXP} - T_i^{CAL}\right)^2}{N})^{1/2}$
RMSD (y_i)	$(\sum_{i=1}^{N} \frac{\left(Y_i^{EXP} - Y_i^{CAL}\right)^2}{N})^{1/2}$
AAD (T_i)	$\sum_{i=1}^{N} \left\|T_i^{EXP} - T_i^{CAL}\right\| /N$
AAD (y_i)	$\sum_{i=1}^{N} \left\|Y_i^{EXP} - Y_i^{CAL}\right\| /N$

Table A13. The boiling points of the components at pressures of 1.0 kPa and 50.0 kPa.

System	P/kPa	Boiling Point/K
n-hexanol	1.0	328.15
n-octanol	1.0	356.05
	50.0	442.60
n-dodecane	1.0	358.90
	50.0	461.85
n-tridecane	1.0	373.35
	50.0	479.90
n-octanol/n-dodecane (Azeotropic Point)	1.0	351.05
	50.0	443.45

Table A14. Estimation parameters of the distillation columns.

Operation Parameter	T1	T2	T3	T4	T5
Operating pressure/kPa	1.0	1.0	1.0	1.0	50.0
Number of theoretical plates	35	40	35	40	45
Feed entrance point	15	18	15	18	20
Distillate flow rate/kg/h	980.0	80.0	197.0	297.086	217.086
Reboiler heat duty/kW	309.73	108.95	137.59	63.78	64.59
Total heat duty/kW			684.64		

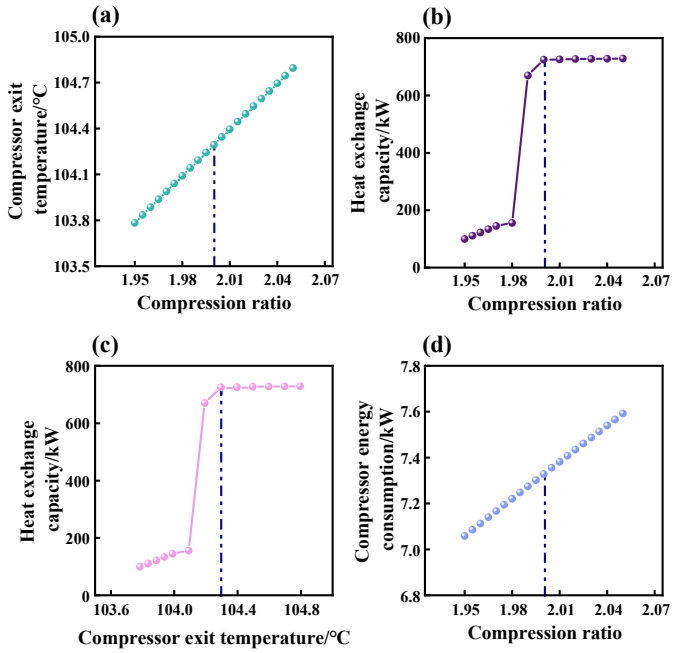

Figure A1. Sensitivity analysis of compressor 2. (**a**) Compression ratio versus compressor exit temperature.; (**b**) Compression ratio versus heat- exchange capacity.; (**c**) Compressor exit temperature versus heat- exchange capacity.; (**d**) Compression ratio versus compressor energy consumption.

References

1. Chen, Y.; Zhou, M.-J.; Hu, Y.; Xie, Y. Direct hydrogenation of natural oils to fatty alcohols enabled by an alcoholysis/hydrogenation relay strategy and two-phase solvent system. *Org. Biomol. Chem.* **2024**, *22*, 6703–6707. [CrossRef]
2. Kabangu, M.J.; Lubbe, S.J.; Crouse, P.L. Extraction and Separation of Zirconium Using 1-Octanol. *Min. Metall. Explor.* **2020**, *37*, 93–100. [CrossRef]
3. Almi, S.; Bouzgou, M.; Adjal, F.; Barkat, D. Methyl-isobutyl ketone and 1-octanol as synergistic agents and phase modifiers in solvent extraction of cobalt(II) by the N-(2-hydroxybenzylidene)aniline from sulfate medium. *Inorg. Nano-Met. Chem.* **2019**, *50*, 8–15. [CrossRef]
4. Ampronpong, W.; Suren, S.; Mohdee, V. Experimental and DFT investigations on the supramolecular mechanism of Ni(II) extraction via D2EHPA blended 1-octanol extractant: Application of vegetable oils as diluents. *Korean J. Chem. Eng.* **2023**, *40*, 594–611. [CrossRef]
5. Duan, W.-Y.; Qin, Y.-L.; Zhang, S.-B. Inhibitory Mechanisms of Plant Volatile 1-Octanol on the Germination of *Aspergillus Flavus* Spores. *Food Biophys.* **2023**, *19*, 96–108. [CrossRef]
6. Jackson, A.S.M.; Goberdhan, D.; Dowding, P.J.; Roberts, K.J. Data for crystallisation of a homologous series of single and mixed n-alkanes (C_{16}–C_{23}) from representative hydrocarbon fuel solvents. *Data Brief* **2023**, *48*, 109198. [CrossRef]
7. Wang, J.; Sun, L.; Luan, P. Effect of diesel blended with di-*n*-butyl ether/1-octanol on combustion and emission in a heavy-duty diesel engine. *Environ. Pollut.* **2022**, *311*, 119976. [CrossRef]
8. Wang, M.; Song, E.; Li, L.; Zhang, Y.; Wang, E. Application of dividing wall column in azeotropic distillation with intermediate boiling-point heteroazeotrope: Simulation and optimization. *Chem. Eng. Res. Des.* **2022**, *189*, 384–400. [CrossRef]
9. Yin, K.; Liu, T.; Dai, Y.; Li, G. A new correlation model of entrainer properties and process economics for ternary azeotrope separation by extractive distillation. *Process Saf. Environ. Prot.* **2023**, *177*, 711–724. [CrossRef]
10. Wang, W.; Yang, Q.; Xu, H.; Wang, Y. Effects of separation sequences on the reactive distillation coupled with extractive distillation under different pressures. *Chem. Eng. Sci.* **2024**, *300*, 120604. [CrossRef]
11. Zhang, Z.; Wang, Y.; Zhang, M.; Guang, C.; Li, M.; Gao, J. Energy-saving investigation of pressure-swing distillation strengthening configurations for benzene/isobutanol binary azeotrope. *Sep. Purif. Technol.* **2022**, *296*, 121381. [CrossRef]
12. Wu, H.; Ye, Q.; Li, J.; Xu, Z.; Pan, J. Novel energy-efficient designs of heterogeneous azeotropic distillation for separating ternary organic wastewater based on self-heat recuperation technology. *Process Saf. Environ. Prot.* **2024**, *183*, 1038–1050. [CrossRef]
13. Shan, B.; Wang, S.; Xu, Q. Design and multi-objective optimization of hybrid extractive distillation process for separating the toluene-methanol-water ternary azeotrope. *Sep. Purif. Technol.* **2024**, *336*, 126335. [CrossRef]
14. Bonthuys, G.J.K.; Schwarz, C.E.; Burger, A.J.; Knoetze, J.H. Separation of alkanes and alcohols with supercritical fluids. Part I: Phase equilibria and viability study. *J. Supercrit. Fluids* **2011**, *57*, 101–111. [CrossRef]
15. Mukeba, O.H.; Motang, N.; Schwarz, C.E. Mixtures of supercritical CO_2 + (1-octanol and/or *n*-alkanes) at saturation: Density and viscosity measurements. *J. Supercrit. Fluids* **2025**, *225*, 106672. [CrossRef]
16. Díaz, I.; Palomar, J.; Rodríguez, M.; de Riva, J.; Ferro, V.; González, E.J. Ionic liquids as entrainers for the separation of aromatic–aliphatic hydrocarbon mixtures by extractive distillation. *Chem. Eng. Res. Des.* **2016**, *115*, 382–393. [CrossRef]
17. Sun, Y.; Han, P.; Tian, X.; Wang, R.; Wang, H.; Li, C.; Liu, J. Process design and thermal integration for efficient separation of alpha-bisabolol via vacuum distillation. *Sep. Purif. Technol.* **2025**, *367*, 132830. [CrossRef]
18. Parsana, V.M.; Parikh, S.; Ziniya, K.; Dave, H.; Gadhiya, P.; Joshi, K.; Gandhi, D.; Vlugt, T.J.H.; Ramdin, M. Isobaric Vapor-Liquid Equilibrium Data for Tetrahydrofuran + Acetic Acid and Tetrahydrofuran + Trichloroethylene Mixtures. *J. Chem. Eng. Data* **2023**, *68*, 349–357. [CrossRef]
19. Freire, N.V.; Nunes, M.C.; Arce, P.F. Vapor-liquid equilibrium for the {R-OH + R-palmitate} systems at 50.3 and 101.3 kPa. *Fuel* **2022**, *333*, 126459. [CrossRef]
20. Chen, Q.; Gu, L.L.; Zhang, Z.H. The Binary Vapor-Liquid Phase Equilibrium of Citronella Oil under High Vacuum. *Adv. Mater. Res.* **2013**, *772*, 281–286. [CrossRef]
21. Barbieri, C.; Guido, G.D.; Moioli, S. Vapor-liquid equilibrium data for the binary system isopropanol+water at 60 kPa and 80 kPa. *J. Chem. Thermodyn.* **2024**, *198*, 107342. [CrossRef]
22. Batutah, M.A.; Kuswandi, K.; Wibawa, G. Isobaric Binary Vapor–Liquid Equilibrium of Ethanol + Glycerol and 1-Propanol + Glycerol Systems at 16.0 and 101.3 kPa. *J. Chem. Eng. Data* **2020**, *65*, 3802–3807. [CrossRef]
23. Frisch, M.; Trucks, G.; Schlegel, H.B.; Scuseria, G.E.; Robb, M.; Cheeseman, J.R.; Scalmani, G.; Barone, V.; Petersson, G.A.; Nakatsuji, H.; et al. *Gaussian 16 Revision. A. 03*; Gaussian Inc.: Wallingford, CT, USA, 2016.
24. Shi, K.; Wang, R.; Wang, H.; Li, C.; Liu, J. Heat-pump distillation and dividing wall column processes for 1,4-butanediol purification. *Sep. Purif. Technol.* **2025**, *379*, 134960. [CrossRef]
25. Shi, K.; Zheng, H.; Sun, Y.; Wang, H.; Fang, J.; Li, C.; Liu, J. Vapor-liquid equilibrium for 1,4-butanediol, ethylene glycol and 3-methyl-1,5-pentanediol systems under different vacuum conditions. *Vacuum* **2024**, *230*, 113752. [CrossRef]

26. An, Y.; Li, W.; Li, Y. Design/optimization of energy-saving extractive distillation process by combining preconcentration column and extractive distillation column. *Chem. Eng. Sci.* **2015**, *135*, 166–178. [CrossRef]
27. Qi, J.; Li, Y.; Xue, J.; Qiao, R. Comparison of heterogeneous azeotropic distillation and energy-saving extractive distillation for separating the acetonitrile-water mixtures. *Sep. Purif. Technol.* **2019**, *238*, 116487. [CrossRef]
28. Douglas, J.M. *Conceptual Design of Chemical Processes*; McGraw-Hill: New York, NY, USA, 1988.
29. Rao, J.; Tian, X.; Sun, Y.; Wang, H.; Wang, R.; Li, C.; Liu, J. Molecular mechanism based extractant screening and process design for the separation of 2-methyltetrahydrofuran-acetonitrile azeotrope. *Chem. Eng. Sci.* **2025**, *320*, 122445. [CrossRef]
30. Li, Q.; Feng, Z.; Rangaiah, G.P.; Dong, L. Process Optimization of Heat-Integrated Extractive Dividing-Wall Columns for Energy-Saving Separation of CO_2 and Hydrocarbons. *Ind. Eng. Chem. Res.* **2020**, *59*, 10721–11098. [CrossRef]
31. Seider, W.D.; Lewin, R.D.; Seader, J.D.; Widagdo, S.; Gani, R.; Ng, K.M. *Product and Process Design Principles: Synthesis, Analysis and Evaluation*; John Wiley & Sons Inc.: New York, NY, USA, 2004.
32. Gao, X.; Yang, Y.; Chen, M.; Cheng, Q.; Lu, K. Novel heat pump reactive distillation and dividing-wall column reactive distillation processes for synthesizing isopropyl acetate to save TAC and reduce CO_2 emissions. *Chem. Eng. Process.-Process Intensif.* **2022**, *171*, 108746. [CrossRef]
33. Li, J.; Zhou, D.; Yang, W. A multi-component reaction mechanism of n-butanol, n-octanol, and di-n-buthylether for engine combustion. *Fuel* **2020**, *275*, 117975. [CrossRef]
34. Gadalla, M.A.; Olujic, Z.; Jansens, P.J.; Jobson, M.; Smith, R. Reducing CO_2 emissions and energy consumption of heat-integrated distillation systems. *Environ. Sci. Technol.* **2005**, *39*, 6860–6870. [CrossRef]
35. Waheed, M.A.; Oni, A.O.; Adejuyigbe, S.B. Performance enhancement of vapor recompression heat pump. *Appl. Energy* **2014**, *114*, 69–79. [CrossRef]
36. Keating, L.; Harris, H.H.; Chickos, J.S. Vapor pressures and vaporization enthalpy of (−) α-bisabolol and (*dl*) menthol by correlation gas chromatography. *J. Chem. Thermodyn.* **2017**, *107*, 18–25. [CrossRef]
37. Zhao, Q.; Wang, H. Measurement and Correlation of the Isobaric Vapor–Liquid Equilibria of Methanol + Dimethyl Carbonate + 1-Butyl-3-Methylimidazolium Hexafluorophosphate at 101.3 kPa. *J. Chem. Eng. Data* **2023**, *68*, 2529–2750. [CrossRef]
38. Bharadwaj, B.R.; Kumar, K.R.; Kommagalla, P.K.; Palagummi, D.K.; Satyavathi, B. Measurement and Correlation Studies of Phase Equilibria and Thermophysical Properties of 2,6-Dichlorotoluene. *J. Chem. Eng. Data* **2024**, *68*, 2599–2609. [CrossRef]
39. de Klerk, D.L.; Schwarz, C.E. Simplified Approach to Understanding, Evaluating, and Parameterizing the NRTL Model for the Description of Binary VLE: Τττ-VLE Approach. *Ind. Eng. Chem. Res.* **2023**, *62*, 10629–10643. [CrossRef]
40. Xing, C.-H.; Wu, Y.-Y.; Wu, B.; Chen, K.; Ji, L.-J. Vapor–Liquid Equilibrium for the Binary Systems Involving Cumene, *t*-Butylbenzene, and *sec*-Butylbenzene at 101.3 kPa. *J. Chem. Eng. Data* **2024**, *69*, 1026–1033. [CrossRef]
41. Madeira, P.P.; Xu, X.; Wu, Y.-T. Liquid−Liquid Equilibrium of Aqueous Polymer Two-Phase Systems Using the Modified Wilson Equation. *Ind. Eng. Chem. Res.* **2005**, *55*, 1247–1251. [CrossRef]
42. Modk, G.; Lang, P. Removal and Recovery of Organic Solvents from Aqueous Waste Mixtures by Extractive and Pressure Swing Distillation. *Ind. Eng. Chem. Res.* **2012**, *51*, 11473–11481. [CrossRef]